Local lattice structure in Mn-doped $La_{2-x}Sr_xCuO_4$ studied by Cu and Mn *K*-edge XAFS

C. J. Zhang,[1] H. Oyanagi,[1,*] B. H. Kim,[2] Y. W. Park,[2] and Y. H. Zhang[3]
[1]*National Institute of Advanced Industrial Science and Technology, 1-1-1 Umezono, Tsukuba 305-8568, Japan*
[2]*School of Physics and Nano Systems Institute-National Core Research Center, Seoul National University, Seoul 151-747, Korea*
[3]*Structure Research Laboratory, University of Science and Technology of China, Hefei 230026, People's Republic of China*
(Received 23 August 2006; revised manuscript received 29 November 2006; published 7 May 2007)

The local lattice structures in Mn-doped $La_{2-x}Sr_xCuO_4$ are investigated by Cu *K*-edge and Mn *K*-edge x-ray-absorption near-edge structure and extended x-ray-absorption fine structure from 10 to 300 K. The results confirm that the doped Mn ions are located at the Cu site of $La_{2-x}Sr_xCuO_4$ phase and the impurity phases, such as $La_{1-x}Sr_xMnO_3$, are not presented in the samples. It is found that the local lattice structures of Cu are not affected by Mn impurities and the local lattice environments of Mn are similar to those of Cu. We consider that the Mn impurities only break the Cu-O *p-d* hybridization locally, while the local lattice environments and the superconductivity in the regions away from the impurities remain untouched. This result implicates that local lattice inhomogeneity plays an important role in the mechanism of high-temperature superconductivity.

DOI: 10.1103/PhysRevB.75.174504 PACS number(s): 61.10.Ht, 74.62.Dh, 74.81.−g

I. INTRODUCTION

Transition-metal oxides with layered perovskite-type structure have attracted considerable attention due to their exotic structural, electronic, and magnetic properties. These properties are derived from many competing ground states of the complex phase diagram, strong coupling across different energy scales, and the presence of an inhomogeneous texture.[1–5] One consequence of this complexity is that enormous physical property changes can be induced by small chemical and physical perturbations. In high-temperature superconductor, the study of the effects of impurity doping on the electronic and magnetic structures is one of the most useful ways in exploring the mechanism of high-temperature superconductivity.[6–9] It has been found that in cuprate superconductors, small amount of impurity doping at the Cu site leads to severe depression of superconductivity, i.e., only a few percent of impurity (such as Fe, Co, Ni, Zn, Ga, and Al) doping at Cu site results in the complete suppression of superconductivity.[3,10–13] In a naive view, it is believed that the depression of superconductivity in doped cuprates accords with the traditional magnetic pair breaking effect, just like that in type-I superconductors.[10,11,14] However, recently, more and more experimental results indicate that the T_c deviation in Li-, Al-, Zn-, and Ni-doped $La_{2-x}Sr_xCuO_4$ and $YBa_2Cu_3O_{7-\delta}$ is far more complicated; most of these results reveal the importance of local lattice effects on the superconductivity. For example, Ishida *et al.* reported from Al and Cu NMR measurements in Al-doped $La_{1.85}Sr_{0.15}CuO_4$ that the Al impurity induces local moments at neighboring Cu sites, whereas the magnetic property at Cu sites away from an Al impurity is nearly the same as in pure $La_{2-x}Sr_xCuO_4$, indicating that the disturbance by doping Al takes place locally.[15] In a neutron-scattering study, Kimura *et al.* calculated that charge carriers in an area $\pi\xi^2_{ab}$ ($\pi\xi_{ab}\sim 18$ Å) around Zn impurities in $La_{1.85}Sr_{0.15}Cu_{1-x}Zn_xO_4$ are excluded from the superconductivity.[16] These results support a picture that the superconductivity is locally destroyed by the impurities, but it still survives in the regions away from the impurities, which might give a possible explanation for the microscopic coexistence of the superconductivity and the antiferromagnetism, as an inhomogeneous mixture of these two ground states.

Recently, we found a more surprising T_c suppression behavior in studying the effects of Mn doping in $La_{2-x}Sr_xCuO_4$ superconductor. With a few percent of Mn substitution for Cu (less than 6%), we found that the onset critical transition temperature (T_c^{onset}) remains unchanged at about 37 K, while the superconductivity disappears at high Mn doping content.[17–19] This result leads to a more complicated situation in the suppression of superconductivity induced by impurity doping, which should contribute to the understanding of the mechanism of high-temperature superconductivity. However, the unchanged T_c^{onset} is so strange that we must first make sure that the Mn ions are really located at the Cu site in the $Cu(Mn)O_6$ octahedra of K_2NiF_4-type structure. Furthermore, it is of great importance to investigate the local structural effects induced by Mn impurity and its interplay with the superconductivity.

X-ray-absorption near-edge structure (XANES) and extended x-ray-absorption fine structure (EXAFS) are increasingly used in order to determine the local atomic environment around a particular atomic species of sample. As a powerful local structure probe technique, x-ray-absorption spectroscopy (XAS) has been widely exploited to study the cuprate superconductors in order to determine the distribution of local lattice distortions in the electronically active Cu-O networks.[20–26] In recent years, it was found that the local structure distortion and local charge inhomogeneity play an important role in high-temperature superconductivity. Based on the above facts, in this paper, we report a detailed analysis of the local lattice structures in Mn-doped $La_{2-x}Sr_xCuO_4$ by both Cu *K*-edge and Mn *K*-edge XANES and EXAFS studies.

II. EXPERIMENT

It is well known that the Mn ions tend to exist at +3 or +4 valence states in perovskite oxides (such as K_2NiF_4-type manganite $La_{1-x}Sr_{1+x}MnO_4$ and ABO_3-type $La_{1-x}Sr_xMnO_3$).

Since the nominal valence state of Cu ions in $La_{2-x}Sr_xCuO_4$ is believed to be only slightly higher than +2, the substitution of Cu by high-valent Mn would lead to rapid decrease of nominal hole concentration, which consequently leads to the valence mismatch in this system. As the result, it is difficult to obtain pure phase $La_{1.85}Sr_{0.15}Cu_{1-x}Mn_xO_4$ samples at higher Mn doping level. In fact, we find impurity phases in $La_{1.85}Sr_{0.15}Cu_{1-x}Mn_xO_4$ at $x>0.1$.[18] However, since the valence state of Sr (+2) is lower than that of La^{3+}, one can expect that simultaneous change of the Sr and Mn concentrations can partially compensate the valence mismatch induced by Mn doping. Using this technique, we have successfully synthesized high-quality single phase $La_{1.85-y}Sr_{0.15+y}Cu_{1-x}Mn_xO_4$ samples at high Mn doping level. In this study, $La_{1.875-1.5x}Sr_{0.125+1.5x}Cu_{1-x}Mn_xO_4$ $(0\leqslant x\leqslant 0.2)$ polycrystalline samples are synthesized by means of a conventional solid-state reaction method and the detailed procedure has been described elsewhere.[17–19] The Sr concentration in the parent compound $La_{1.875}Sr_{0.125}CuO_4$ is slightly lower than the optimal concentration of $x=0.15$. The reason for choosing the Sr concentration of $0.125+1.5x$ is based on two facts: One is that the increasing of Sr concentration, with increasing Mn doping will nominally compensate the valence mismatch induced by Mn doping and avoid the rapid decrease of charge carrier concentration, and the other is that one can check the T_c value at different Mn and Sr contents. The weighted powder was mixed and preheated at 1150 to 1180 °C for several times. Then, the powder is pressed into pellets and sintered at the same temperature for 24 h. It should be mentioned that low-temperature preheat tends to form impurity phase which should be avoided. X-ray-diffraction analysis indicates that all samples are formed in a single phase within resolution limits. Resistivity as a function of temperature was measured using a standard four-probe method in a closed-cycle helium cryostat. All XAS measurements were performed in a fluorescence detection mode at BL13B, Photo Factory. A novel Ge pixel array detector (PAD) with 100 segments was used in order to gain high throughput and energy resolution, and as a result, high signal-to-noise Mn *K*-edge x-ray-absorption spectroscopies for dilute Mn-doped samples are achieved. The detailed description of PAD apparatus was reported elsewhere.[27] Samples are mounted on an aluminum holder and attached to a closed-cycle helium refrigerator. The holder rotates on a high-precision goniometer (Huber 420) to change the incidence angle. The incidence angle is 15° with respect to the sample surface for Cu *K*-edge XAS experiments and 12° for Mn *K*-edge XAS experiments. These specific angles are chosen in order to decrease the self-absorption effect in fluorescence signal and avoid the diffraction.

III. RESULTS AND DISCUSSION

Figure 1 shows the temperature dependence of resistivity for $La_{1.875-1.5x}Sr_{0.125+1.5x}Cu_{1-x}Mn_xO_4$ $(0\leqslant x\leqslant 0.2)$ samples. From Fig. 1, one can see that the resistivity of Mn-free sample with $x=0$ decreases with decreasing temperature. It exhibits superconducting transition at about 28.5 K, and zero resistivity is found at about 22.8 K. The broad transition

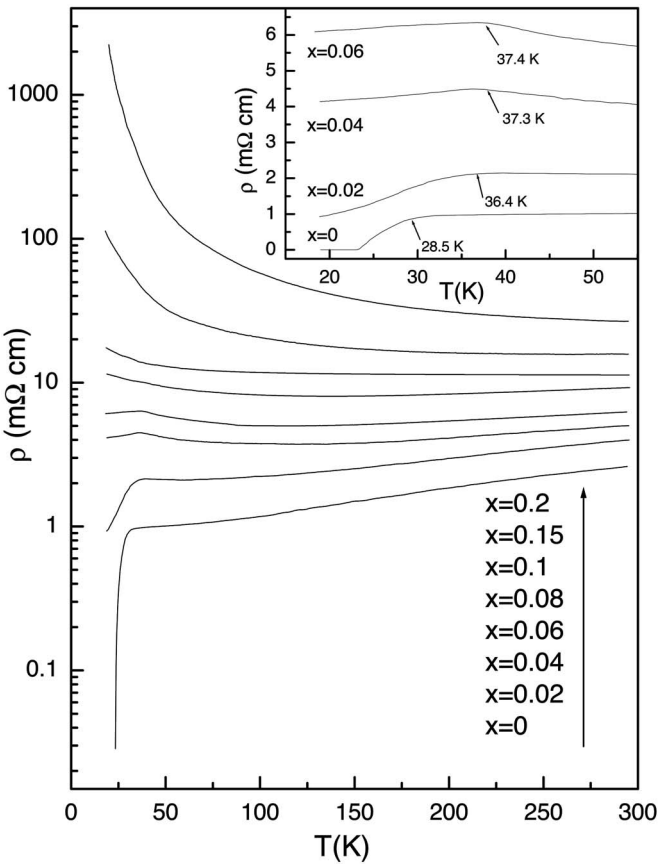

FIG. 1. Temperature dependence of resistivity for $La_{1.875-1.5x}Sr_{0.125+1.5x}Cu_{1-x}Mn_xO_4$ $(0\leqslant x\leqslant 0.2)$ samples. The inset shows the enlarged view near the transition temperature.

width ΔT_c (~6 K) may come from the grain-boundary effects in bulk polycrystalline sample. The resistivity normally increases with increasing Mn doping. The increase of resistivity should be related to the perturbation of hybridization of Cu $3d$ orbitals and O $2p$ orbitals induced by Mn impurities. However, as one can see from the inset of Fig. 1, the resistivity shows a subtle drop at about 37 K in $x=0.02$, 0.04, and 0.06 samples, which is related to the superconducting transition. The decrease of resistivity becomes weaker as the Mn doping content is increased, which indicates that the superconducting volume decreases with increasing Mn doping. Similar behavior of Mn doping effects in $La_{1.85}Sr_{0.15}CuO_4$ superconductor has been reported in our previous studies.[17–19] The drop of resistivity at about 37 K indicates that the superconducting transition occurs at higher temperature in Mn-doped samples than that in $x=0$ sample, even though the superconducting transition lasts in a wider temperature range. We consider that the simultaneous change of Sr and Mn dopings leads to the change of the resistivity behavior. The Mn doping introduces impurities into the CuO_2 plane, which results in the increase of resistivity. However, the increasing of Sr content results in the increase of onset superconducting transition temperature. This drop of resistivity is consistent with our previous reports that the T_c^{onset} value keeps at about 37 K with a few percent of Mn doping in $La_{1.85}Sr_{0.15}CuO_4$. The anomalous behavior in Mn-

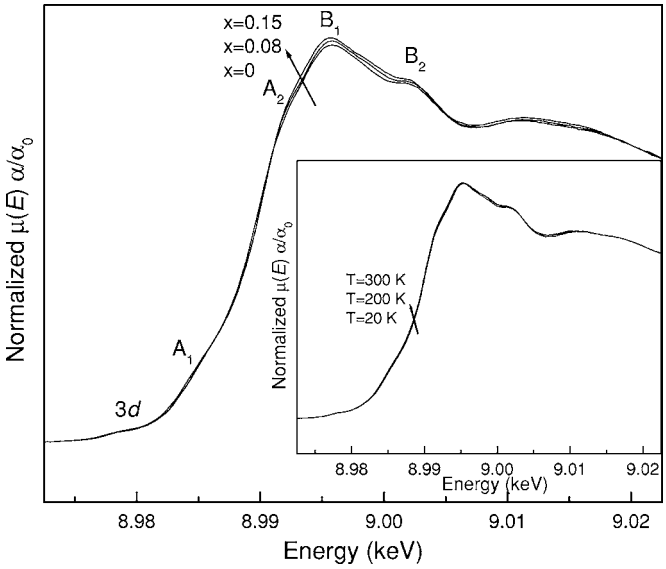

FIG. 2. Normalized Cu K-edge XANES spectra at room temperature for $La_{1.875-1.5x}Sr_{0.125+1.5x}Cu_{1-x}Mn_xO_4$ for $x=0$, 0.08, and 0.15 samples. The inset shows the normalized Cu K-edge XANES spectra for $x=0.15$ at several representative temperatures.

doped $La_{2-x}Sr_xCuO_4$ superconductor obviously contradicts with previous reports where the T_c value decreases rapidly with a few percent of impurities doping at Cu site.[3,10–13]

The anomalous behavior in Mn-doped samples is quite interesting as it should certainly be related to the principle mechanism of high-temperature superconductivity. However, it is well known that another type of perovskite manganite oxide, $La_{1-x}Sr_xMnO_3$, can be formed under similar synthesizing environments, i.e., higher than 1000 °C in air. Thus, it is crucial to investigate whether the doped Mn ions are formed in K_2NiF_4-type structure and whether the Mn ions are located at the Cu site or not. Furthermore, it is of great importance to investigate the effects of Mn doping on the local lattice structure of the $La_{2-x}Sr_xCuO_4$ superconductors. In order to solve these uncertainties, we performed systematical studies of Cu K-edge XAFS and Mn K-edge XAFS of $La_{1.875-1.5x}Sr_{0.125+1.5x}Cu_{1-x}Mn_xO_4$ from room temperature to low temperature. Figure 2 shows normalized Cu K-edge XANES spectra at room temperature for $La_{1.875-1.5x}Sr_{0.125+1.5x}Cu_{1-x}Mn_xO_4$. The spectra display the usual characteristic features observed in Cu K-edge XANES spectra of cuprates. As the samples are polycrystalline, the absorption feature contains the information of both in-plane and out-of-plane structures. In Fig. 2, the energy positions of characteristic features (A_1, A_2, B_1, and B_2) observed within 30 eV above the weak $1s$-$3d$ transition peak are indicated. The A_1 and A_2 features are due to the $1s$-$4p^*(\pi)$ transition, while B_1 and B_2 are assigned to the $1s$-$4p^*(\sigma)$ transition. The absorption feature of Mn-doped samples are similar to that of Mn-free sample, which means that the doping of Mn does not lead to any structural changes or any valence variation of Cu. In the inset of Fig. 2, we show the temperature dependence of normalized Cu K-edge XANES for $x=0.15$ sample. The energy shift with decreasing temperature is very small (less than 0.1 eV), which indicates that no structural phase

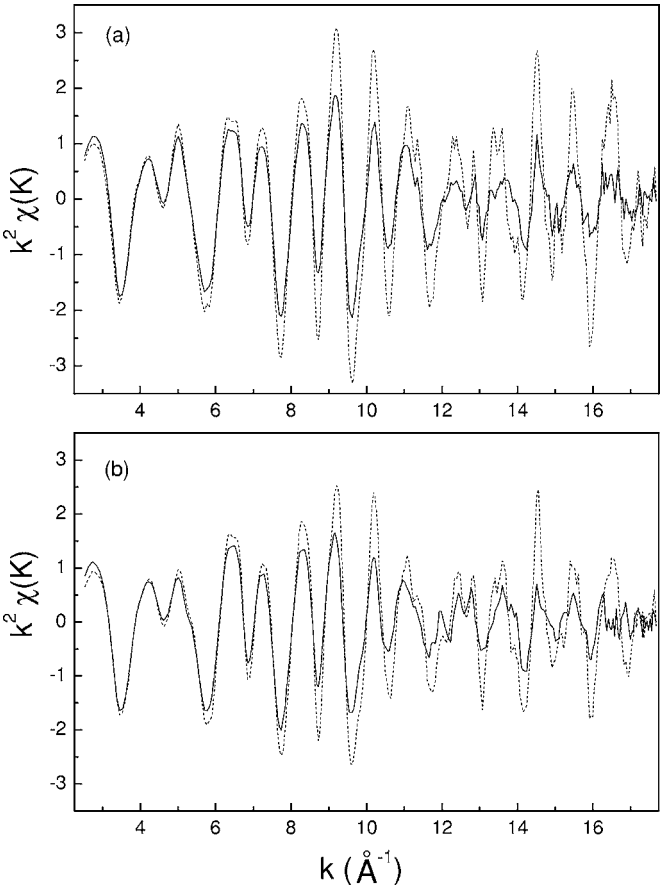

FIG. 3. Cu K-edge EXAFS signal multiplied by k^2 measured on $La_{1.875-1.5x}Sr_{0.125+1.5x}Cu_{1-x}Mn_xO_4$ samples at 300 K (solid line) and 30 K (dashed line) for (a) $x=0$ and (b) $x=0.15$.

transitions or valence evolutions occur with decreasing temperature.

Figure 3 gives representative examples of the Cu K-edge EXAFS oscillations (weighted by k^2) extracted from the measured absorption on the $La_{1.875-1.5x}Sr_{0.125+1.5x}Cu_{1-x}Mn_xO_4$ samples at 300 and 30 K for (a) $x=0$ and (b) $x=0.15$, respectively. The absorption threshold ($k=0$) is set to 8980.3 eV, E_F of Cu metal. One can find that the magnitude of the oscillations increases at higher k region as temperature is decreased, in accordance with dynamic lattice disorder (uncorrelated phonons). This indicates that the oxygen displacement suffers from a lattice disorder effect in both Mn-free sample and Mn-doped samples. Figures 4(a) and 4(b) show the Fourier transforms $|\mathrm{FT}(k^2\chi(k))|$ of the EXAFS oscillations (weighted by k^2) of the $x=0$ and $x=0.15$ samples at several representative temperatures. The k-dependent profile of total oscillation reflects the weighted sum of scattering amplitude functions of La(Sr), Cu(Mn), and O. The first peak in the Fourier transform (FT) corresponds to the in-plane Cu-O atoms, while the doublet peak structure at around 3–4 Å corresponds to the Cu-La(Sr) and Cu-O-Cu multiple-scattering signals. The small peaks located at the 2–3 Å range come from the contribution of Cu-O (apical) bonds and local CuO_6 octahedral distortions. The peaks of Cu-O, Cu-La(Sr), and Cu-O-Cu scattering signals show strong temperature dependence, i.e., the FT ampli-

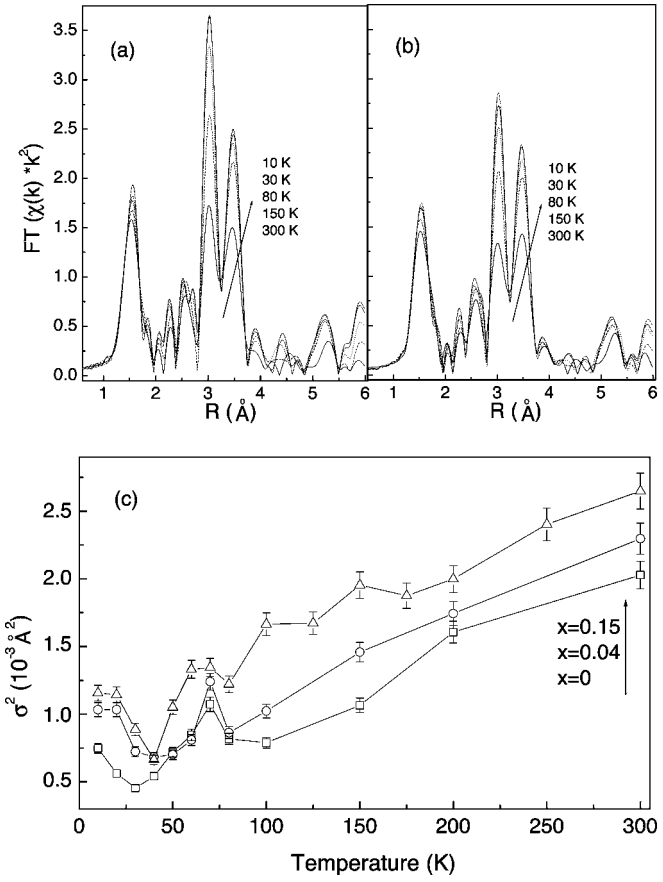

FIG. 4. [(a) and (b)] Fourier transforms of the EXAFS oscillations (weighted by k^2) of the $x=0$ and $x=0.15$ samples at several representative temperatures. (c) The temperature dependence of Cu-O (planer) Debye-Waller factor for $x=0$, 0.04, and 0.15 samples.

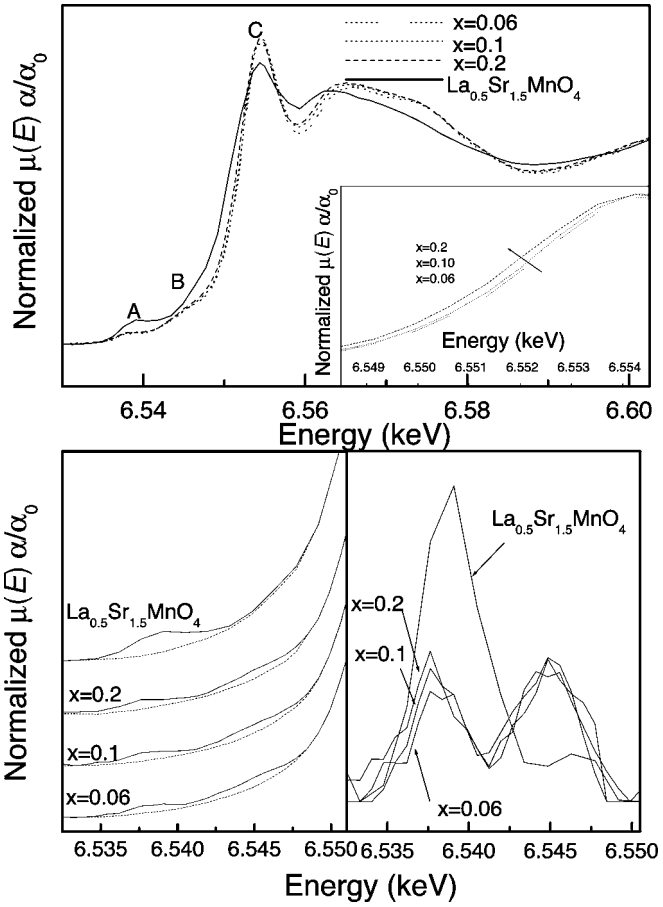

FIG. 5. Upper panel: normalized Mn *K*-edge XANES spectra for $La_{1.875-1.5x}Sr_{0.125+1.5x}Cu_{1-x}Mn_xO_4$ polycrystalline samples with $0.06 \leqslant x \leqslant 0.2$ and $La_{0.5}Sr_{1.5}MnO_4$ single-crystal sample. For the single-crystal sample, the incidence beam is arranged so that the electric-field vector **E** of the synchrotron radiation is parallel to the *ab* plane. The inset shows the enlarged view of the absorption edge region. Lower left panel: an expanded view of the pre-edge of Mn *K*-edge spectra. The dashed lines are the background approximations to guide the eyes. The background-subtracted pre-edge features vs energy are given in the lower right panel.

tudes increase with decreasing temperature. It is noticeable that both the feature and the temperature-dependent amplitude of the Fourier transforms are similar for the $x=0$ and $x=0.15$ samples. The EXAFS signals of the Cu-O bonds are well separated from the longer bond contributions and have been extracted by the standard Fourier filtering method. The filtered EXAFS signals represent single backscattering of the photoelectron emitted at the Cu site by its nearest-neighbor oxygens and therefore probe the correlation function between Cu and oxygen pairs. Multiple-scattering signals, which make the data analysis more complex, are excluded in this analysis because such signals have a longer effective photoelectron path length. Individual EXAFS data ($k < 18$ Å^{-1}) for the nearest-neighbor Cu-O_p correlations are filtered and curve fitted in k space using a single-scattering formula with theoretical phase-shift functions calculated by FEFF6. Structural parameters such as the in-plane Cu-O_p distance $R_{\text{Cu-O}}$ and mean-square relative displacement of oxygens $\sigma_{\text{Cu-O}}$ relative to copper ions are determined. This approach is adopted to make a direct comparison of the local lattice distortions of the Mn-doped samples with the Mn-free sample, where the correlated Debye-Waller factor (DWF) of the Cu-O pairs is the suitable order parameter of local CuO_2 displacements. Within experimental uncertainties, the $R_{\text{Cu-O}}$ value is found to be temperature independent and similar to that determined by diffraction study ($R_{\text{Cu-O}} \sim 1.885$ Å). The temperature dependence of correlated DWF of Cu-O pairs is shown in Fig. 4(c) for $x=0.15$, $x=0.04$, and $x=0$ samples. At high temperature, the Debye-Waller factor decreases with decreasing temperature, which is due to the weakening of thermally fluctuation-induced oxygen displacement. A noticeable feature is that the temperature-dependent DWF displays an upturn at temperature below 80 K. This upturn is a common feature in the temperature dependence of DWF of cuprate superconductors.

Figure 5 gives the normalized Mn *K*-edge XANES spectra for $La_{1.875-1.5x}Sr_{0.125+1.5x}Cu_{1-x}Mn_xO_4$ samples with $0.06 \leqslant x \leqslant 0.2$. In order to compare the local environments of Mn ions, we also plot the normalized in-plane Mn *K*-edge XANES spectrum for $La_{0.5}Sr_{1.5}MnO_4$ single crystal in the same figure. The $La_{0.5}Sr_{1.5}MnO_4$ sample is the same as the one used previously.[28] The arrangement of the incidence beam used to measure the x-ray-absorption spectroscopy of

single crystal with the electric-field vector **E** is parallel to the *ab* plane (**E**∥*ab*). It is found that the XANES spectra of $La_{1-x}Sr_{1+x}MnO_4$ exhibit anisotropic feature, i.e., the spectra show difference between in-plane and out-of-plane components regarding their spectral shape or the absorption edge positions. The powder spectra (nonpolarized) recorded in fluorescence mode is found to be well reproduced by the weighted sum (2/3:1/3) of the polarized in-plane and out-of-plane spectra.[29] For the $La_{0.5}Sr_{1.5}MnO_4$ single crystal, the energy difference in the position of the absorption edge between both polarizations is very small and the absorption edge of a powder $La_{0.5}Sr_{1.5}MnO_4$ is identical to the absorption edge of the polarized in-plane spectra. From Fig. 5, we notice that the absorption thresholds of $La_{1.875-1.5x}Sr_{0.125+1.5x}Cu_{1-x}Mn_xO_4$ samples are higher in energy compared to that of $La_{0.5}Sr_{1.5}MnO_4$. This results may give an evidence that the nominal valence state of Mn in $La_{1.875-1.5x}Sr_{0.125+1.5x}Cu_{1-x}Mn_xO_4$ samples is slightly higher than 3.5, taking into account that the nominal valence state of Mn in $La_{0.5}Sr_{1.5}MnO_4$ is +3.5. However, the quantitative determination of the valence state of Mn is not allowed from XANES spectra. The low intensity pre-edge region, which roughly extends from 6535 to 6550 eV, shows a double-peak feature (labeled as A and B) in both $La_{0.5}Sr_{1.5}MnO_4$ and $La_{1.875-1.5x}Sr_{0.125+1.5x}Cu_{1-x}Mn_xO_4$ samples. In the lower left panel of Fig. 5, an expanded view of the pre-edge of Mn *K*-edge spectra is given. The dashed lines are the background approximations to guide the eyes. In order to have a closer view on the double-peak feature, the background-subtracted pre-edge features vs energy for these samples are given in the lower right panel. It is noticeable that the double-peak feature has similar magnitude in the nonpolarized $La_{1.875-1.5x}Sr_{0.125+1.5x}Cu_{1-x}Mn_xO_4$ powder samples. However, feature A is much stronger in the *ab*-plane spectra of $La_{0.5}Sr_{1.5}MnO_4$ in which feature B is much weaker. This gives an implication that feature A is more related to the *ab* plane and feature B is more likely related to out-of-plane spectra.[30] It can be noticed that the prepeak feature is smeared in $La_{1.875-1.5x}Sr_{0.125+1.5x}Cu_{1-x}Mn_xO_4$ samples compared to that in $La_{0.5}Sr_{1.5}MnO_4$, which is consistent with the fact that the Mn ions are dilutedly distributed in the $Cu(Mn)O_2$ plane in $La_{1.875-1.5x}Sr_{0.125+1.5x}Cu_{1-x}Mn_xO_4$ samples.

Figure 6(a) gives the corrected Mn *K*-edge EXAFS oscillation for $La_{1.875-1.5x}Sr_{0.125+1.5x}Cu_{1-x}Mn_xO_4$ with $x=0.15$ at 300 and 10 K. The absorption threshold ($k=0$) is set to 6539.1 eV, the first inflection point of the pure Mn foil. The Mn *K*-edge EXAFS oscillation spectra are similar to that of Cu *K*-edge EXAFS oscillation spectra of $La_{2-x}Sr_xCuO_4$, but different from the Mn *K*-edge EXAFS oscillation spectra of $La_{1-x}Sr_xMnO_3$.[31,32] This result further confirms that Mn ions are doped at the Cu site in $La_{2-x}Sr_xCuO_4$ phase and it does not form $La_{1-x}Sr_xMnO_3$ phase in these samples. In order to rule out the possibility of Mn impurities taking the La site, we make a comparison of a simulated Mn *K*-edge EXAFS oscillation of the Mn-O pair assuming that Mn ions are taking the La site with the experimental EXAFS oscillation of the first shell, as shown in Fig. 6(b). It can be seen that the deviation between experimental data and the simulation is large, which confirms that Mn ions are not taking the La site.

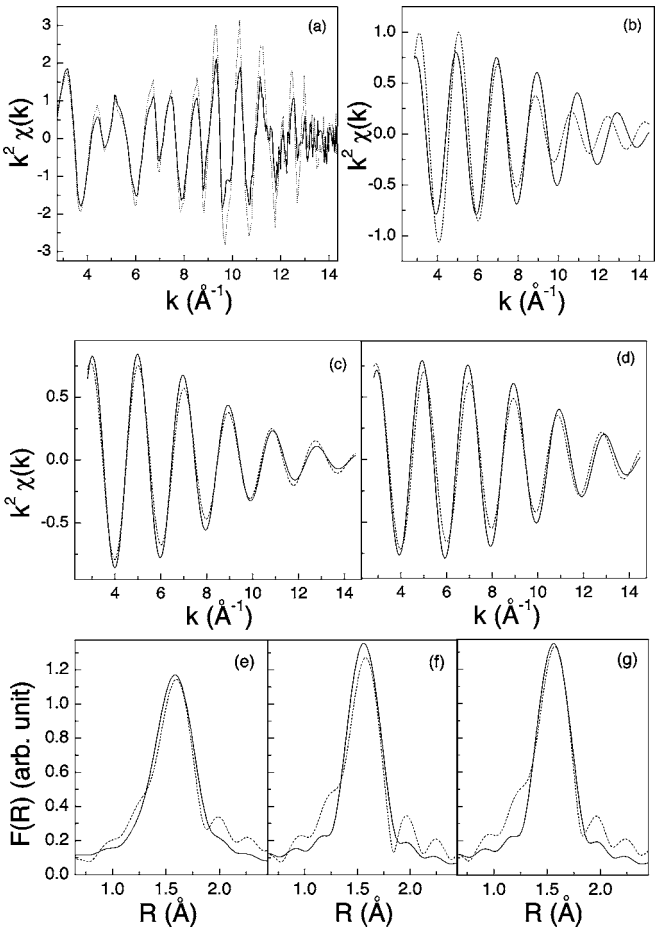

FIG. 6. (a) The Mn *K*-edge EXAFS oscillation for $La_{1.875-1.5x}Sr_{0.125+1.5x}Cu_{1-x}Mn_xO_4$ with $x=0.15$ at 300 K (solid line) and 10 K (dotted line); (b) comparison of the simulated Mn *K*-edge EXAFS oscillation assuming that Mn takes La site (dashed line) with the experimental oscillation of the first shell (solid line); and (c) and (d) are experimental isolated Mn-O contributions to the Mn *K*-edge EXAFS oscillation at 300 and 10 K, respectively (solid lines). Theoretical fitting based on a Gaussian RDF of Mn-O bonds are shown as dashed lines. (e) and (f) are Fourier transform magnitude curves for the nearest-neighbor Mn-O_p correlation at 300 and 10 K, respectively. Experimental curves are indicated by solid lines, and dashed lines indicate Fourier transform results for theoretical EXAFS curves based on a single-scattering formula and theoretical phase-shift functions. (g) Fourier transform magnitude curves for the nearest-neighbor Mn-O_p correlation at 10 K using two-site model (dashed line) and comparison with experimental curves (solid line).

We conclude that the Mn ions are formed in a $La_{2-x}Sr_xCuO_4$-type phase and they take Cu site. The magnitude of the oscillations increases at higher *k* region as temperature is decreased, which indicates that the dynamic lattice disorder (or oxygen displacement) around Mn atoms is significant at low temperature, similar to the Cu *K*-edge oscillation in $La_{2-x}Sr_xCuO_4$. To proceed with the characterization of the Mn-O bond distribution, the nearest-neighbor Mn-O_p is fitted using a single-Gaussian Mn-O radial distribution function (RDF). The phase shifts are calculated using FEFF6 codes and the lattice parameters of a $La_{0.5}Sr_{1.5}MnO_4$

single crystal are used with Mn ions located at the center of the unit cell. The fitting results for $x=0.15$ sample based on a single-Gaussian RDF of Mn-O bonds are shown in Figs. 6(c) and 6(e) for the EXAFS oscillation at 300 K and Fig. 6(d) and 6(f) for 10 K. It should be noted that the peaks in the FT do not represent the real atomic distances, and the position should be corrected for the photoelectron backscattering phase shifts to find the quantitative value of the atomic positions with respect to the central Mn. From Figs. 6(c) and 6(e), one can see that a single-Gaussian fit nearly agrees with the experimental data at 300 K with Mn-O bond length $r=1.9158$ Å, suggesting that the Mn ions are well crystallized in a $La_{2-x}Sr_xCuO_4$ phase. The Mn-O_p RDF is also analyzed by a mean-square relative displacement for a particular ij pair σ_{ij}^2. The $\sigma_{\text{Mn-O}}^2$ value at 300 K is 0.001 998 Å^2, which is in good agreement with the $\sigma_{\text{Cu-O}}^2$ value in $La_{2-x}Sr_xCuO_4$, suggesting that the Mn ions are well substituted under MnO_6 octahedral environments.[22–24] However, fits to the $x=0.15$ sample at 10 K using a single-Gaussian Mn-O RDF show disagreement with the experimental data [as shown in Figs. 6(d) and 6(f)]. Note the increased deviation between the Gaussian RDF fit and data at high values of k ($k>10$ Å) in Fig. 6(d). To explain the deviation between the Gaussian RDF fit and data at low temperature, the two-site parabolic potential was chosen as the simplest model beyond a single harmonic site model.[21,26] The Fourier transform magnitude curves for the nearest-neighbor (NN) Cu-O_p correlation using two-site model with two NN distance of 0.1 Å is shown in Fig. 6(g) as a dashed line. It is found that the two-site model fits well the experimental curve (solid line). The detailed analysis of Mn K-edge EXAFS oscillation indicates that not only the doped Mn ions are located at the Cu site in a $La_{2-x}Sr_xCuO_4$ phase, but also the local environments of Mn are similar to that of Cu, despite of a small elongation of Mn-O bond length compared to the Cu-O bond length of $r=1.885$ Å.

Now, let us have a brief discussion on the local lattice structure of the Mn-doped system based on the Cu and Mn K-edge EXAFS results. From Fig. 4(c), we notice that the temperature dependence of DWF exhibits an upturn at about 80 K, both in the superconducting samples and in the nonsuperconducting sample. This upturn of DWF indicates that a certain kind of dynamic lattice distortion occurs below this temperature, which leads to local lattice and charge inhomogeneities. The lattice and charge inhomogeneities are observed in different cuprate superconductors by various experimental methods. The mechanisms of the inhomogeneity are proposed in different models assuming a specific distortion type, i.e., Q_2-type Jahn-Teller distortion,[33,34] low-temperature tetragonal distortion,[21] anti-Jahn-Teller distortion,[35] etc. In order to clarify the mechanism, further studies of various experiments using different materials and comparison between theory and experiment are needed. In the Mn-doped samples, the upturn in the temperature dependence of the Debye-Waller factor indicates that the introduction of Mn impurities does not destroy the intrinsic lattice distortion in the CuO_2 plane of this system. However, since the Mn ions are introduced as impurities, these impurities certainly destroy the inherent lattice environments around them. The introduction of Mn impurities may give additional disorder around them and may influence the neighboring Cu sites. Thus, it is natural that the Debye-Waller factor is slightly larger in Mn-doped samples than that in Mn-free sample. According to these two facts, we consider that the effects of Mn are limited to the vicinity of Mn impurities while the local lattice distortion (or a certain kind of phonon) away from the Mn impurities remains intact. Since the superconductivity occurs in a cuprate but not in a manganite, the superconductivity will certainly be destroyed at least in the vicinity of the Mn impurities. Based on these facts, we can explain the different way of the suppression of superconductivity in Mn-doped system (undecreased T_c^{onset} in the Mn-doped samples). The anomalous suppression of superconductivity in Mn-doped $La_{2-x}Sr_xCuO_4$ superconductor can thus be explained in terms of the charge inhomogeneity scenario.[36] In $La_{2-x}Sr_xCuO_4$ superconductor, a small amount of Mn doping leads to the destruction of the superconductivity in its vicinity, while the superconductivity in the regions away from the Mn impurities remains intact. Since the superconductivity is destroyed in the vicinity of Mn, the superconducting volume decreases with the introduction of Mn, which is evidenced by the gradual decrease of the Meissner volume with increasing Mn doping.[17–19] As the effects of Mn impurities are limited to the in vicinity, the local lattice environments away from impurities remain intact and the superconducting transition temperature is not reduced, in contrast to the rapid decrease of transition temperature in other impurity doping conditions (such as Zn, Ni, Fe, etc.). The superconductivity disappears when the Mn impurities are too excessive and bulk superconductivity is suppressed.

In spite of the fact that the majority thought that high-temperature superconductivity in cuprates is dominated by an electronic mechanism, pure electronic models on a homogeneous conducting plane are strongly challenged by recent experimental results which give increasing evidences of intrinsic electronic inhomogeneity in cuprate superconductors. The recent observations of the kink behavior by angle-resolved photoelectron spectroscopy,[37] and the unconventional isotope effects by muon-spin rotation,[38,39] give evidences that phonons are vital components of the phenomenon through the unconventional electron-phonon coupling. It has been suggested that the charge inhomogeneity governs the behavior of the superconducting phase coherence and the transition to the superconducting state at T_c.[36,40] In the present case, the doped Mn ions not only steadily locate at the Cu site in a $La_{2-x}Sr_xCuO_4$ phase but also have little influence on the local lattice inhomogeneity in the regions away from them (as evidenced by the remaining of the upturn and the drop in Cu-O pair DWF in Mn-doped samples). However, the introduction of Mn impurities destroys the superconductivity in local areas and decreases the superconducting fraction. With increasing Mn doping, the superconducting fraction decreases and eventually the superconductivity disappears. The most striking point in the Mn-doped case is that the Mn impurities only suppress the superconductivity near them, while they do not affect the superconductivity in the regions away from them. This reveals the inhomogeneous character of high-temperature superconductivity, and the lattice and charge inhomogeneities play an important role in the occurrence of superconductivity. It also

gives a sign that the pairing mechanism of high-temperature superconductivity is of short-range nature.

IV. CONCLUSION

In summary, systematical XAFS studies on the local environments of Cu ions and Mn ions in Mn-doped $La_{2-x}Sr_xCuO_4$ reveal that the Mn ions are undoubtedly located at the Cu site in a K_2NiF_4-type structure. In contrast to the rapid decrease of T_c value in Ni and Zn doping cases, the doped Mn impurities do not suppress the superconducting transition in the conventional way. The detailed XAFS analysis indicates that the local lattice environments of both Cu and Mn are nearly the same in both Mn-free and Mn-doped LSCO superconductors. The results support the scenario that the local lattice and charge inhomogeneities play an important role in the mechanism of superconductivity.

ACKNOWLEDGMENTS

The authors express their thanks to the Phonon Factory staff for their supports in XAFS experiments. This work was partially supported by Japan Society for the Promotion of Science (JSPS).

*Electronic address: h.oyanagi@aist.go.jp

[1] N. Tsuda, K. Nasu, A. Yanase, and K. Siratori, *Electronic Conduction in Oxides* (Springer, Berlin, 1991).
[2] Hans B. Brom and J. Zaanen, in *Handbook of Magnetic Materials*, edited by K. H. J. Buschow (Elsevier, Amsterdam, 2003), Vol. 12.
[3] H. Harashina, T. Nishikawa, T. Kiyokura, S. Shamoto, M. Sato, and K. Kakurai, Physica C **212**, 142 (1993).
[4] S. A. Kivelson, E. Fradkin, and V. J. Emery, Nature (London) **393**, 550 (1998).
[5] J. Orenstein and A. J. Millis, Science **288**, 468 (2000).
[6] J. M. Tranquada, B. J. Sternlieb, J. D. Axe, Y. Nakamura, and S. Uchida, Nature (London) **375**, 561 (1995).
[7] J. M. Tranquada, J. D. Axe, N. Ichikawa, A. R. Moodenbaugh, Y. Nakamura, and S. Uchida, Phys. Rev. Lett. **78**, 338 (1997).
[8] K. Fujita, T. Noda, K. M. Kojima, H. Eisaki, and S. Uchida, Phys. Rev. Lett. **95**, 097006 (2005).
[9] W. Meevasana, N. J. C. Ingle, D. H. Lu, J. R. Shi, F. Baumberger, K. M. Shen, W. S. Lee, T. Cuk, H. Eisaki, T. P. Devereaux, N. Nagaosa, J. Zaanen, and Z.-X. Shen, Phys. Rev. Lett. **96**, 157003 (2006).
[10] J. M. Tarascon, L. H. Greene, P. Barboux, W. R. McKinnon, G. W. Hull, T. P. Orlando, K. A. Delin, S. Foner, and E. J. McNiff, Phys. Rev. B **36**, 8393 (1987).
[11] G. Xiao, M. Z. Cieplak, J. Q. Xiao, and C. L. Chien, Phys. Rev. B **42**, 8752 (1990).
[12] Y. Fukuzumi, K. Mizuhashi, K. Takenaka, and S. Uchida, Phys. Rev. Lett. **76**, 684 (1996).
[13] F. Rullier-Albenque, H. Alloul, and R. Tourbot, Phys. Rev. Lett. **91**, 047001 (2003).
[14] Leonid A. Openov, Phys. Rev. B **58**, 9468 (1998).
[15] K. Ishida, Y. Kitaoka, K. Yamazoe, K. Asayama, and Y. Yamada, Phys. Rev. Lett. **76**, 531 (1996).
[16] H. Kimura, M. Kofu, Y. Matsumoto, and K. Hirota, Phys. Rev. Lett. **91**, 067002 (2003).
[17] C. Zhang and Y. Zhang, Phys. Rev. B **68**, 054512 (2003).
[18] C. Zhang, J. S. Kim, B. H. Kim, and Y. W. Park, Int. J. Mod. Phys. B **19**, 303 (2005).
[19] H. Huang, M. Tan, C. Zhang, and Y. Zhang, Physica C **421**, 56 (2005).
[20] S. D. Conradson and I. D. Raistrick, Science **243**, 1340 (1989).
[21] A. Bianconi, N. L. Saini, A. Lanzara, M. Missori, T. Rossetti, H. Oyanagi, H. Yamaguchi, K. Oka, and T. Ito, Phys. Rev. Lett. **76**, 3412 (1996).
[22] N. L. Saini, H. Oyanagi, Z. Wu, and A. Bianconi, Supercond. Sci. Technol. **15**, 349 (2002).
[23] N. L. Saini, H. Oyanagi, A. Lanzara, D. Di Castro, S. Agrestini, A. Bianconi, F. Nakamura, and T. Fujita, Phys. Rev. B **64**, 132510 (2001).
[24] N. L. Saini, H. Oyanagi, V. Scagnoli, T. Ito, K. Oka, and A. Bianconi, Europhys. Lett. **63**, 125 (2003).
[25] N. L. Saini and H. Oyanagi, Physica C **412**, 152 (2004).
[26] J. Mustre de Leon, M. Acosta-Alejandro, S. D. Conradson, and A. R. Bishop, J. Synchrotron Radiat. **12**, 193 (2005).
[27] H. Oyanagia, C. Fonne, D. Gutknecht, P. Dressler, R. Henck, M.-O. Lampert, S. Ogawa, K. Kasai, and S. B. Mohamed, Nucl. Instrum. Methods Phys. Res. A **513**, 340 (2003).
[28] Y. Murakami, H. Kawada, H. Kawata, M. Tanaka, T. Arima, Y. Moritomo, and Y. Tokura, Phys. Rev. Lett. **80**, 1932 (1998).
[29] J. Herrero-Martín, J. García, G. Subías, J. Blasco, and M. C. Sánchez, Phys. Rev. B **72**, 085106 (2005).
[30] H. Oyanagi (unpublished).
[31] T. Shibata, B. A. Bunker, and J. F. Mitchell, Phys. Rev. B **68**, 024103 (2003).
[32] N. M. Souza-Neto, A. Y. Ramos, H. C. N. Tolentino, E. Favre-Nicolin, and L. Ranno, Phys. Rev. B **70**, 174451 (2004).
[33] G. Grüner, *Density Wave in Solids*, Frontiers in Physics Vol. 89 (Addison-Wesley, Reading, MA, 1994).
[34] B. I. Kochelaev, J. Sichelschmidt, B. Elschner, W. Lemor, and A. Loidl, Phys. Rev. Lett. **79**, 4274 (1997).
[35] A. Bussmann-Holder and H. Keller, Eur. Phys. J. B **44**, 487 (2005).
[36] D. Mihailovic, V. V. Kabanov, and K. A. Müller, Europhys. Lett. **57**, 254 (2002).
[37] A. Lanzara, P. V. Bogdanov, X. J. Zhou, S. A. Kellar, D. L. Feng, E. D. Lu, T. Yoshida, H. Eisaki, A. Fujimori, K. Kishio, J.-I. Shimoyama, T. Noda, S. Uchida, Z. Hussain, and Z.-X. Shen, Nature (London) **412**, 510 (2001).
[38] R. Khasanov, D. G. Eshchenko, H. Luetkens, E. Morenzoni, T. Prokscha, A. Suter, N. Garifianov, M. Mali, J. Roos, K. Conder, and H. Keller, Phys. Rev. Lett. **92**, 057602 (2004).
[39] A. Bussmann-Holder, H. Keller, A. R. Bishop, A. Simon, R. Micnas, and K. A. Müller, Europhys. Lett. **72**, 423 (2005).
[40] D. Mihailovic, Phys. Rev. Lett. **94**, 207001 (2005).